

THE USE OF HHG AT 4GLS

B.W.J. McNeil, SUPA, Department of Physics, University of Strathclyde, Glasgow, UK
 D. Dunning and N.R. Thompson, ASTeC, CCLRC Daresbury Laboratory, UK
 B. Sheehy, Sheehy Scientific Consulting, New York, USA.

Abstract

4GLS is a facility proposed for the Daresbury Laboratory in the UK which will offer users a suite of high brightness synchronised sources from THz frequencies into the XUV [1]. In the current design, photon energies from 8-100eV will be generated in a variable polarisation FEL amplifier directly seeded by a High Harmonic Gain system. The reasoning behind this choice will be discussed and characterisation of the sources based on the present design presented.

INTRODUCTION

The Conceptual Design Report for the 4GLS project to be based at UK's Daresbury Laboratory has been published [1]. A suite of synchronised coherent variably polarised radiation sources covering the spectrum from THz frequencies to photons energies of ~ 100 eV will provide the scientific community with a tool that will enable new windows of scientific exploration to be opened and thereafter exploited. Initially, the major themes of the 4GLS science programme will lie in time-resolved measurements and nanoscience. Details of the science case driving the need for 4GLS were first published in [2] and more recently updated in [1].

A major component of 4GLS will be the XUV-FEL. The current design for this component is for a seeded FEL amplifier that operates in the 8-100 eV photon energy range to provide peak powers between approximately 1-10 GW allowing very high field intensities of up to 10^{17} W/cm² to be achieved. In order to tune over the spectral range both the electron beam energy and the undulator magnetic field are variable. Because the FEL acts as an amplifier the seed sources also need to be continuously tunable.

There are several potential benefits in operating a FEL as an amplifier of an injected seed as opposed to allowing the FEL to self-seed from inherent noise to generate Self Amplified Spontaneous Emission. An important benefit is the potential improvement in the temporal coherence of the FEL output over that of SASE. This increases the spectral brightness. Shot-to-shot reproducibility and stability are also improved. The amplified pulse width, being determined by that of the seed, may be significantly shorter than that of the electron pulse, and indeed there is the potential to amplify more exotic pulses for post-amplification manipulation. Finally, the length of FEL interaction required to achieve saturation may be shortened, thereby reducing space requirements and ultimately costs. All of these bene-

fits require that the seed power be significantly greater than the spontaneous power due to the inherent noise.

XUV-FEL OVERVIEW

The design of the 4GLS XUV-FEL has undergone several iterations [3]..[6]. The XUV-FEL branch of the 4GLS conceptual design is shown in schematic form in Fig. 1. Typical operating parameters and specification for the conceptual design are given in Table 1.

Table 1: XUV-FEL conceptual design parameters

General	
FEL design	High Gain Amplifier
Seeding mechanism	HHG source
Photon output	
Tuning Range	$\sim 8 - 100$ eV
Peak Power	$\sim 8 - 2$ GW
Repetition rate	~ 1 kHz
Polarisation	Variable elliptical
Min Pulse length FWHM	< 50 fs
Typical $\Delta f \Delta t$	~ 0.6
Max pulse energy	$400 \mu\text{J}$
Electron beam parameters	
Energy	750 - 950 MeV
Bunch Charge	1 nC
RMS bunch length	266 fs
Normalised emittance	2π mm mrad
RMS energy spread	0.1%
Undulator parameters	
Undulator Type	PPM & APPLE-II
No of Modules	8 & 5
Module lengths	~ 2 m
Period	45 mm & 51 mm
Focusing	FODO
Minimum magnetic gap	~ 10 mm

The work of [6] describes some detail of the undulator and focusing lattice choices based upon studies using the design formulae of Xie [7] and steady state 3-D simulations using Genesis [8]. Undulator module lengths of ≈ 2 m were chosen with a simple FODO quadrupole focusing lattice inserted between modules along with BPMs and phase matching units. This solution requires a shorter total undulator length to achieve saturation than the longer module options considered in [5], which require a more complex quadrupole doublet or triplet focusing system. However,

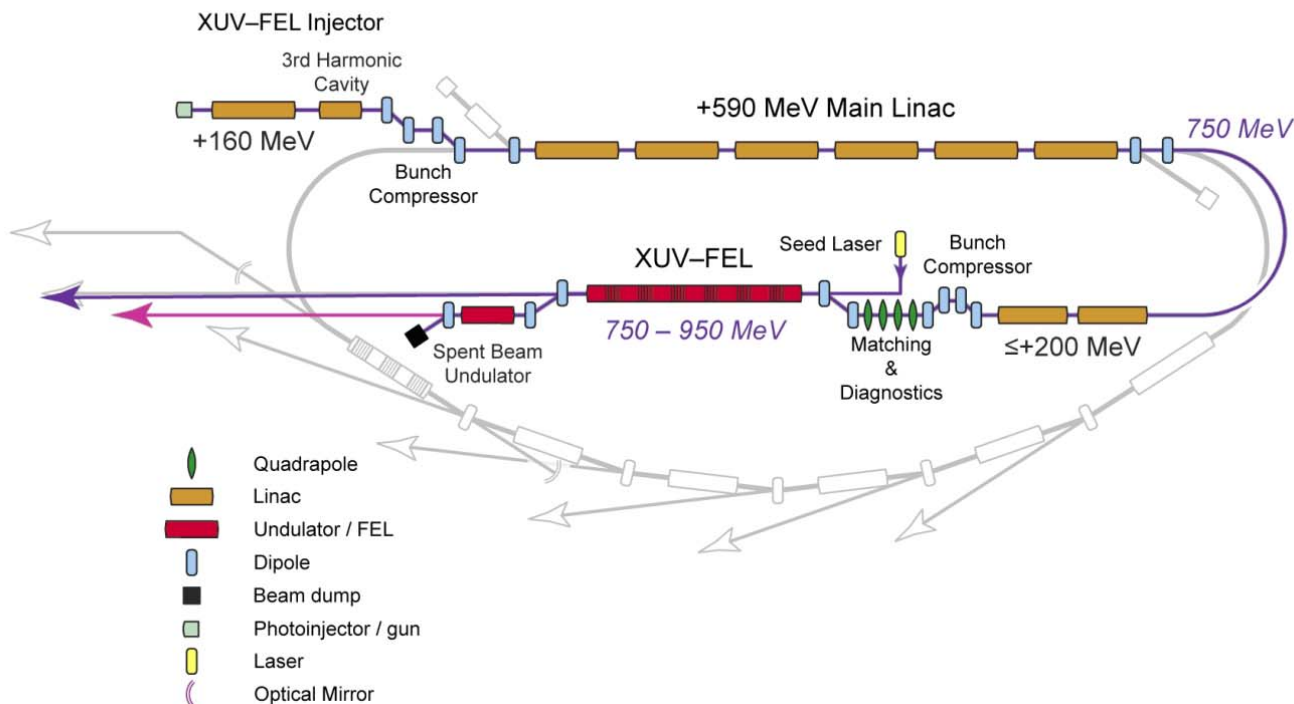


Figure 1: Schematic layout of the XUV-FEL conceptual design.

when gaps between modules are included, the total overall length of modules plus gaps is slightly longer for the shorter module option. The ability to monitor and optimise the electron beam transverse position at regular intervals to ensure optimal radiation-electron beam coupling throughout the FEL and the relative simplicity of the design ensured the shorter 2 m module length with FODO focusing was chosen.

A schematic for the undulator/focusing lattice is shown in Fig. 2. Also shown are the injected radiation seed fields focused to the beginning of the first resonant undulator module, for each of the cases. The undulator length is therefore controlled so that saturation always occurs in the final variable undulator module VU5. In this way, variable polarised photons may be generated across the full operational range of the FEL and it acts as a fixed source simplifying the optical transport system of the output to the final user experimental areas.

It can be seen from Fig. 2 that planar undulator module PU1 is only required to ensure saturation at ~ 100 eV and that its magnetic gap will be at the operational maximum of ~ 28 mm. This module will not be required to operate at gaps very much smaller than this, and therefore the vacuum vessel aperture containing both electron beam and radiation seed can be relatively large at this point. Similar considerations show that module PU2 will operate with minimum magnetic gap slightly smaller again, and so on for the rest of the modules PU3..PU8. Use of a step-tapered

vacuum vessel has therefore been proposed that gradually decreases in aperture from module to module. The two advantages of this approach are that firstly resistive wall and surface roughness wakefields are much reduced compared to a constant minimum aperture, and secondly, as discussed later, the tapered internal aperture allows optimal focusing of the seed pulse across the whole wavelength range.

HIGH HARMONIC GENERATION SOURCES

Peak pulse powers due to intrinsic noise at the beginning of the FEL interaction for the XUV-FEL parameters of Table 1 are typically 30..50 W across the photon energy range 10..100 eV. Any seed source for the XUV-FEL must therefore generate significantly greater power than this if it is to dominate the evolution of the noise to saturation. In addition, these seed sources must be continuously tunable over 10-100 eV. Fortunately, High Harmonic Generation (HHG) sources now exist that meet these seed requirements, or are readily foreseeable within the very near future [1]. Indeed, it can be expected that the rapid advances in this field will be able to easily surpass present 4GLS design requirements for seed sources over the next few years, so this is an area of research that must be closely observed and the XUV-FEL design modified accordingly. Here the method of HHG generation is summarised and the properties of the HHG seed fields described to enable simulation by the 3-D FEL



Figure 2: Schematic of the modular undulator system and focusing lattice of the XUV-FEL demonstrating the different modes of operation across the photon energy range 10-100 eV. Electron beam transport is right to left. Undulator modules marked in grey have large magnetic gaps $\bar{a}_u \approx 0$ and are effectively absent for the purposes of the FEL interaction. The minimum required undulator gap (and vacuum vessel internal aperture) decrease in gradual steps from 28 mm (25 mm) for PU1 down to 10 mm (7 mm) for PU8 and the variable polarisation modules VU1-VU5. Radiation beam waists of the seed and output are shown from 100 eV (violet)..10 eV (red).

code Genesis [8]. Further detail and references regarding the HHG sources systems may be obtained from [1, 9].

The HHG sources are based upon samples of Noble gases driven by a high-energy drive laser [10]. A typical drive laser is a linearly polarised Ti:Sapphire system operating at ~ 800 nm generating several to tens of mJ per pulse of FWHM duration of a few tens of fs. For the 4GLS conceptual design, 14 mJ pulses of width 30 fs FWHM are assumed. The high fields generated by such lasers is the key to harmonic generation. The process can be understood semiclassically at the atomic level in terms of ionization and recombination steps occurring within an optical cycle, with the energy gained by the electron from the laser field between these steps going into the harmonics [11, 12], and the phase of the harmonics being related to the trajectories in the field between steps. By macroscopic phase matching, single trajectory lengths for each harmonic can be selected, and a coherent output, with well-defined phases between the harmonics obtained.

The experimentally observed shape of the HHG yield curve is of a rapid decline of the lower order harmonics followed by a plateau-region, in which the harmonic yield falls relatively slowly. An intensity dependent cut-off harmonic is then reached, beyond which the yield drops quickly to zero [13]. This model is used to construct an HHG field to simulate seed injection into the XUV-FEL in the simulations of later sections - see Fig. 4.

Tuning of the HHG sources may be achieved by suitably modifying the drive laser, for example by introducing a chirp or more generally by adaptive pulse shaping. Contin-

uous tuning between adjacent harmonics is possible above about the 25th harmonic or a photon energy of ~ 40 eV (31 nm). Below this photon energy it is proposed to introduce an intermediate noncollinear phase-matched optical parametric amplifier (NOPA) between Ti:Sapphire laser and the gas, which will give continuously tunable output between 1200 nm to 1475 nm. For the 14 mJ specification of the Ti:Sapphire laser this gives ~ 2 mJ output from the NOPA. Although introducing this further efficiency loss, the system will enable more than sufficient continuously tunable power for XUV-FEL seeding for 8-40 eV operation.

Summarising, the powers available from HHG sources exceed 4GLS requirements. In the XUV-FEL modelling that follows, for 10 eV (100 eV) operation a Gaussian input seed of peak power $P_{pk} = 100$ kW (30 kW) in 30 fs FWHM pulses are assumed. The repetition rate of ~ 1 kHz is well matched to the XUV-FEL seed requirements.

MODELLING SEEDING OF THE XUV-FEL

Seed injection

For effective seeding, the seed pulse should be injected coincident with the electron pulse at the start of the undulator and focused to a waist, w_0 , of approximately the same transverse dimensions as the electron pulse. (The waist minimum w_0 is defined as the radius at which the radiation power is $1/e^2$ of its peak value.) Focusing should not be so tight that the seed diffracts rapidly within a gain length at the start of the FEL interaction (i.e. when the Rayleigh length $Z_R = \pi w_0^2/\lambda \ll L_g$.) The relation for the radiation waist size

$$w(z) = w_0 \sqrt{1 + \left(\frac{z - z_0}{Z_R} \right)^2},$$

where z_0 is the position of the focus along the axis of the undulator lattice, restricts the minimum aperture size of the vacuum vessel that will allow transmission of the seed to its focus. As the focal size is determined by the electron beam radius, which is nearly constant for all seed wavelengths, the vacuum vessel's minimum transverse dimensions are determined by the longest wavelength seed (10 eV photons) which must be focused furthest from the FEL entrance as shown in Fig. 2. As the minimum operational undulator gap decreases with undulator module PU1..PU8, as discussed for Fig. 2, the vacuum vessel may be tapered to accommodate the focusing of the 10 eV photon energy seed. This is demonstrated in Fig. 3, where the seed field is injected at the entrance of undulator module PU1 and focused to the optimal waist (as shown in following simulations) of $w_0 = 200 \mu\text{m}$ at the entrance of module VU1 approximately 21 m downstream. It is seen that the vacuum vessel inner wall dimension at $z = 0$ is 25 mm to accommodate wall thickness and clearance for the 28 mm undulator magnetic gap. The walls are at least two beam

waists away from the peak power on axis at all positions up to the start of the FEL interaction region at $z \approx 21$ m. Thus the tapered vacuum vessel should provide sufficient clearance for injection of this (worst case) 10 eV seed injection.

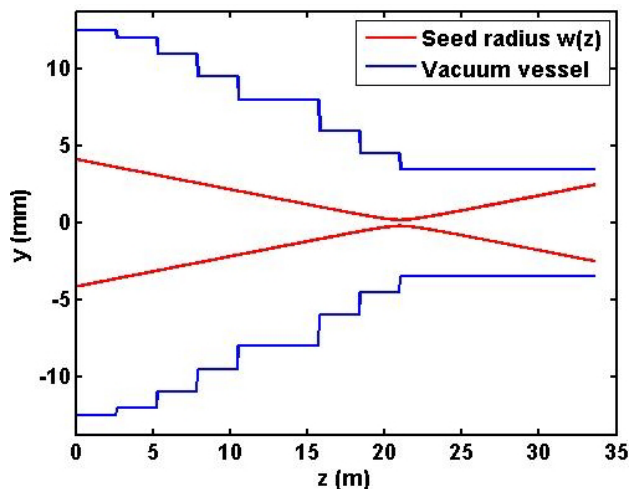


Figure 3: Plot of the dimension of the inner vacuum vessel wall (blue) which has been step-tapered to enable the undulator module tuning ranges of Fig. 2. The waist size $w(z)$ (red) for a 10 eV seed is also shown, focused at the entrance to VU1 at $z = 21$ m.

Seed with full harmonic content

The method of seed generation and specification across the XUV-FEL spectral range is summarised in the previous section and described in more detail in [1, 9]. The HHG seed has interesting spectral and temporal properties, being composed of a large number of narrow, phase-coherent odd harmonics of a fundamental drive laser. This forms a comb structure in frequency-space. Such a phase correlated comb in frequency space has a similar comb-like structure in the temporal domain, resulting in a series of atto-second pulse structures each separated by one half the drive laser period. For a drive laser such as the Ti:Sapphire laser with wavelength of ~ 800 nm, the 65th harmonic corresponds to the maximum XUV-FEL photon energy of 100 eV. If the complete frequency content of a HHG pulse were to be injected into the XUV-FEL it would be preferable if only one of the harmonics, say the n th harmonic, interact resonantly with the electrons. The HWHM gain bandwidth $\Delta\lambda/\lambda \approx \rho$ should then be less than the spacing between harmonics. This gives the condition $\rho < 1/n$. A typical value of $\rho \approx 2 - 3 \times 10^{-3}$ for 100 eV operation so that $\rho < 1/65 \approx 1.5 \times 10^{-2}$ is easily satisfied. Thus, it should be possible to inject all of the seed radiation, including all non-resonant harmonics, into the XUV-FEL without the need for band-pass pre-filtering of the seed, as all non-resonant harmonics will simply become negligible relative to the resonant harmonic as the FEL interaction proceeds through the undulator. For the purposes

of investigating the effects a typical HHG radiation field was generated for use with the 3-D code Genesis. The full HHG spectral power is shown in Fig. 4. However, Gen-

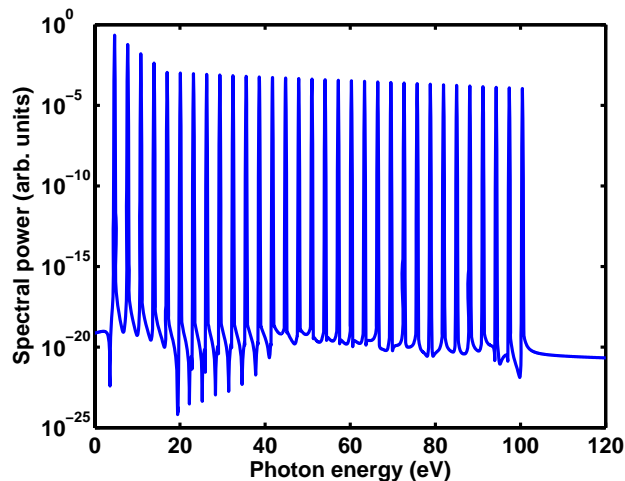


Figure 4: Simulated power spectrum from an HHG source.

esis is a time-averaged code with a minimum interval between sample points of the field of one radiation period so the sampling rate is $\Delta t_s = f_r^{-1}$, the inverse of the resonant frequency. The Nyquist frequency, $f_N = 1/2\Delta t_s$ determines the bandwidth of frequencies that the field can contain without the effects of aliasing. Hence the range of frequencies that can be simulated by Genesis without aliasing effects is $f_r/2 < f_r < 3f_r/2$. Thus from Fig. 4 it is seen that if simulating 100 eV photon energy generation in the XUV-FEL, only the 50-100 eV components of the HHG spectrum should contribute to the Genesis input file using its 'RADFILE' option.

A Genesis simulation was performed for 100 eV operation with the limited spectral range HHG seed pulse as described above. A uniform current of 1.5 kA was assumed. Due to the relatively short slippage experienced at these photon energies, this is very close to that experienced by a short pulse coincident with the Gaussian peak current of the XUV-FEL. All 13 undulator modules were assumed to be the planar type modules PU1..8. The seed at the beginning of the FEL interaction at $z = 0$, the entrance to PU1, is plotted in Fig. 5. Both the atto-second structure in the pulse power and the comb of odd-harmonic wavelengths (inset) are clearly visible. The peak power of the resonant 100 eV (~ 12.3 nm) component is approximately 22 kW.

On propagating through the amplifier to $z = 16.2$ m, Fig. 6 shows that the fine atto-second structure is beginning to be 'washed out' due to the selective amplification of the resonant wavelength at 12.3 nm (inset). All non-resonant harmonics of the seed appear unaffected by the resonant FEL interaction. This is further confirmed by Fig. 7 which shows the output at saturation at $z = 32.4$ m, the end of the interaction region. The radiation pulse shows none of the atto-second structure of the input seed and the spectral power density shows a single high power emission at

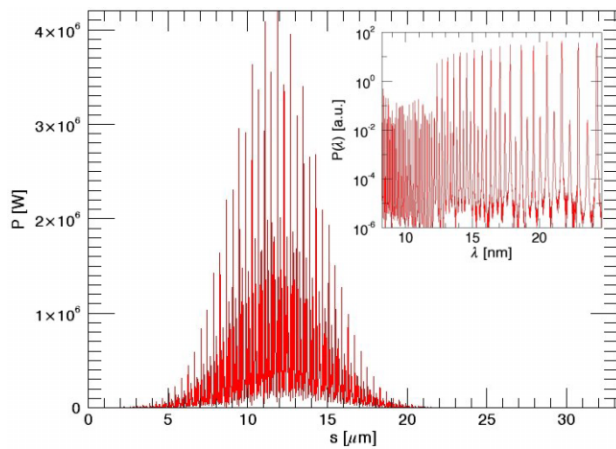


Figure 5: Radiation seed power at the beginning of the amplifier $z = 0$ m as a function of local distance, s . The spectral power content of this pulse is shown as a function of radiation wavelength in the inset.

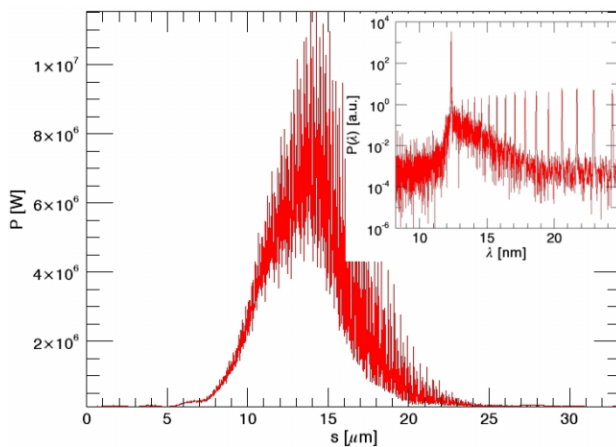


Figure 6: Radiation power as a function of local distance, s , at $z = 16.2$ m through the amplifier. The spectral power content of this pulse is shown as a function of radiation wavelength in the inset.

the resonant wavelength 12.3 nm. It is concluded that, at least for these three-dimensional simulations, the injection of the (Nyquist limited) harmonic content of the HHG seed appears to have no adverse effects in the FEL evolution, or in the saturated emission. The same conclusion may be drawn for lower photon energy XUV-FEL operation where the condition to enable neglect of non-resonant HHG content, $\rho < 1/n$, is more easily satisfied. Thus in all subsequent simulations only the resonant harmonic of the HHG seed content is used in the simulation input.

XUV-FEL 100eV simulations

A complete simulation of the design for the XUV-FEL operating at 100 eV is now demonstrated, using the parameters as given in Table 1. Full details of all parameters may be obtained in [1]. The system modelled is that of Fig. 2

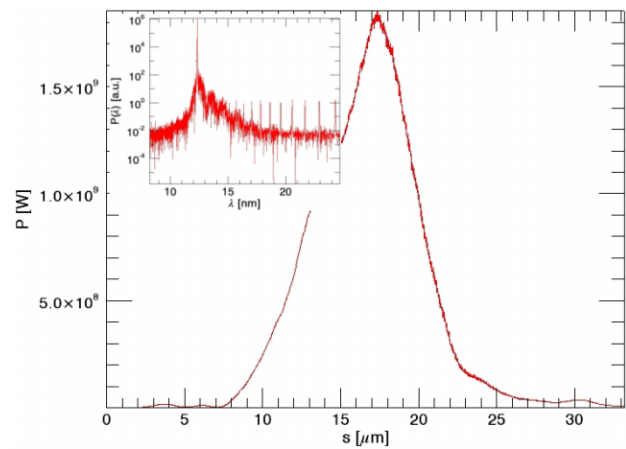


Figure 7: Radiation power as a function of local distance, s , at the end of the amplifier, $z = 32.4$ m. The spectral power content of this pulse is shown as a function of radiation wavelength in the inset.

which, for 100 eV operation, uses the full set of planar and variable undulator modules with the FODO lattice incorporated between modules. The variable APPLE-II undulator modules VU1..5 are set to helical mode so that circularly polarised radiation is generated. The radiation power is plotted in a spatial window that travels along the undulator axis at the speed of light. Fig. 8 plots the power distribution of the seed pulse of peak power $P_{pk} = 30$ kW and duration 30 fs FWHM at the entrance to the first undulator section, PU1. The seed is assumed to have only the resonant har-

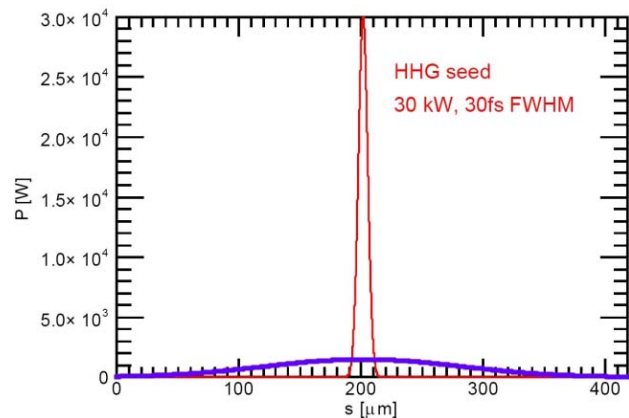


Figure 8: Input radiation seed power (red) to PU1 as a function of local distance, s . The electron beam current profile (blue) is also shown against the same numerical scale.

monic component so that none of the atto-second structure discussed above is present. Also plotted to scale is the electron beam current, here assumed Gaussian, of peak current $I_{pk} = 1.5$ kA and duration 626 fs FWHM. At the exit of the planar undulator modules, it can be seen from Fig. 9 that the peak radiation power has increased to ≈ 70 MW with little change in the pulse structure or width. This pulse

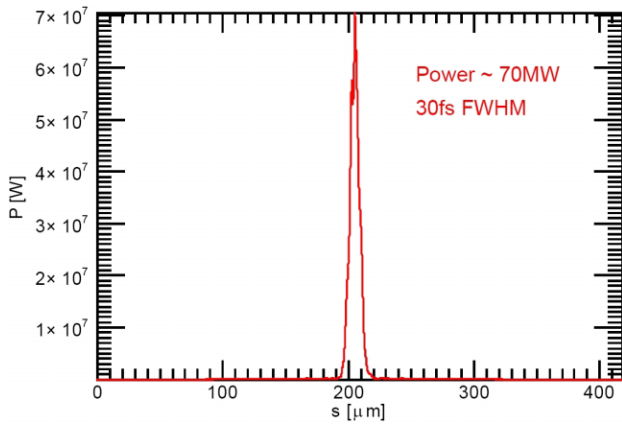


Figure 9: The radiation power at the exit of PU8 as a function of local distance, s .

and the co-propagating electrons are then injected into the set of APPLE-II undulators, VU1 to VU5. By the end of this set of undulator modules, it is seen from Fig. 10 that the FEL interaction has saturated, achieving a peak power of $P_{pk} \approx 2.5$ GW and of duration $\Delta t \approx 60$ fs FWHM. Fourier analysis gives the bandwidth of the spectrum as

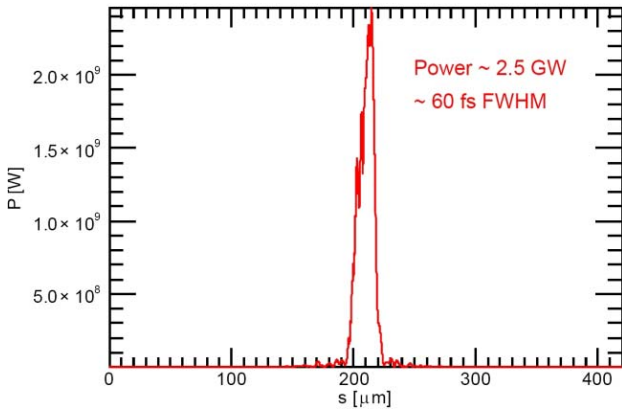


Figure 10: The radiation power at the exit of VU5 as a function of local distance, s .

$\Delta\nu/\nu \approx 5.6 \times 10^{-4}$ which gives a time-bandwidth product of $\Delta f \Delta t \approx 0.8$ which compares favourably with that for a transform limited Gaussian pulse of $\Delta f \Delta t \approx 0.44$. A log-plot of the same data clearly shows in Fig. 11 the relatively clean central seeded region upon a noisier pedestal. This pedestal is the amplified SASE radiation which remains well below saturation because of the smaller initial spontaneous noise radiation (typically a few tens of watts), compared with the initial peak seed power of 30 kW. The shape of the saturated pulse power envelope is not quite as Gaussian as may be expected which suggests that the FEL interaction may have progressed just past saturation. Taking the output power at the end of the previous undulator module, VU4, and plotting it in a similar log plot in Fig. 12, a cleaner Gaussian shape can be seen, with a slightly reduced peak power of $P_{pk} \approx 1.5$ GW. The improved pulse

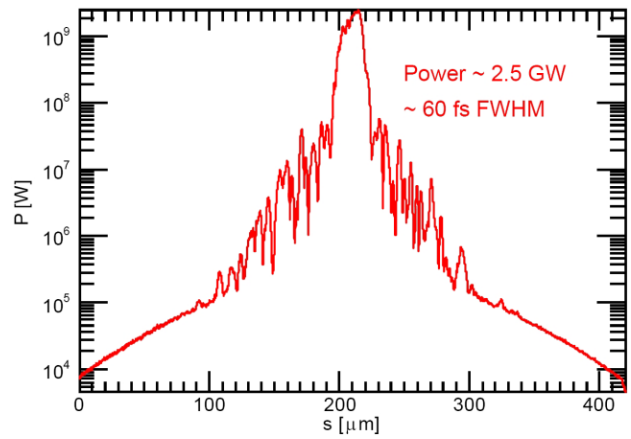


Figure 11: A log-plot of the radiation power at the exit of VU5 as a function of local distance, s .

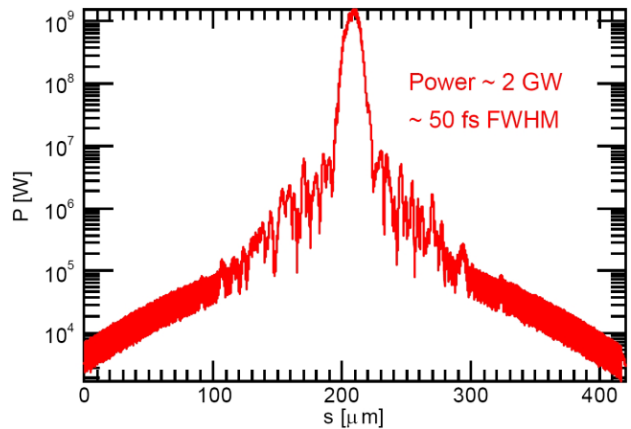


Figure 12: A Log-plot of the radiation power at the exit of VU4 as a function of local distance, s .

shape is confirmed from the pulse duration of $\Delta t \approx 43$ fs FWHM and spectral bandwidth of $\Delta\nu/\nu \approx 6 \times 10^{-4}$ giving an improved time-bandwidth product of $\Delta f \Delta t \approx 0.63$. An improved contrast between the peak power and that of the SASE pedestal is also evident.

XUV-FEL 10eV simulations

Similar simulations to those at 100 eV were carried out for the case of 10 eV operation of the XUV-FEL. Now only the APPLE-II undulator modules VU1 to VU5 are required to achieve saturation as shown schematically in Fig. 2. The input seed power is Gaussian with a peak power $P_{pk} = 100$ kW and duration 30 fs FWHM. The electron pulse current will have the same Gaussian distribution as that for the 100 eV case of Fig. 8.

Radiation power output at the end of undulator module VU5 is shown in Fig. 13 using a log scale. Pulse quality is very good with a peak power of ≈ 6 GW and pulse time-bandwidth product very close to that of a transform-limited Gaussian ($\Delta t \Delta f \approx 0.44$). If the radiation is instead extracted at the end of undulator VU4, the radi-

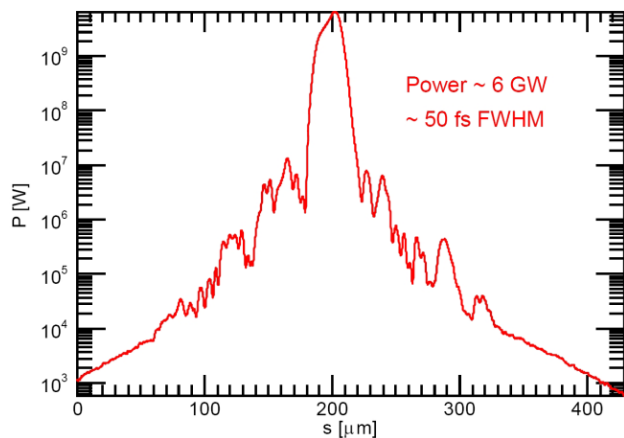


Figure 13: Log-plot of the radiation power for 10 eV operation at the end of undulator module VU5, as a function of local distance, s .

tion power output is shown in Fig. 14. A better contrast

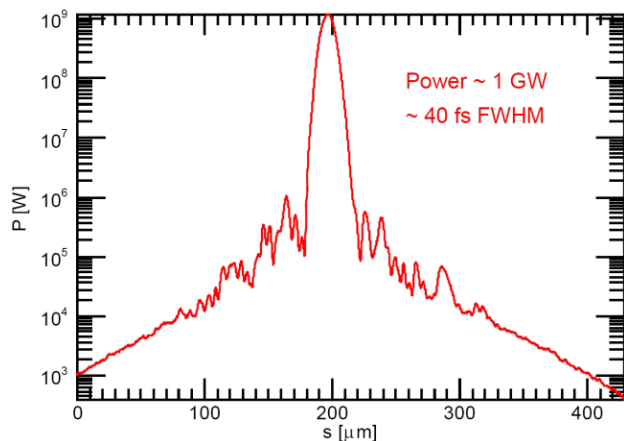


Figure 14: Log-plot of the radiation power for 10 eV operation at the end of undulator module VU4, as a function of local distance, s .

between the peak power of $P_{pk} \approx 1$ GW and the SASE pedestal power is seen from the case of Fig. 13, indicating that the FEL had already saturated before the end of VU5. The time-bandwidth product is approximately the same at $\Delta t \Delta f \approx 0.48$.

Time dependent Genesis 1.3 simulations have also been used to assess the sensitivity of the XUV-FEL output power to the seeding geometry. It is assumed that the most difficult photon energy to achieve optimum geometry will be 10 eV because of the relatively long distance of ≈ 21 m between the seed injection point (before PU1) and the first operational undulator (VU1). The peak seed power of 100 kW was focused to a waist at the beginning of VU1. Fig. 15 shows the effect of varying the size of the focal point waist. An optimum waist of ≈ 200 μm yields a peak output power of $P_{pk} \approx 7.5$ GW. The corresponding Rayleigh length for this focus is ≈ 1.0 m. The Xie formulae [7] estimate the

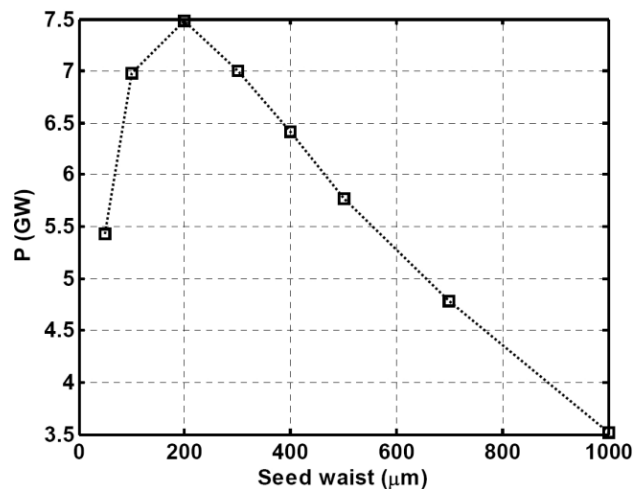


Figure 15: Radiation peak power for 10 eV operation at the end of undulator module VU5, as a function of seed beam waist at the entrance to VU1.

gain length at 10 eV for these parameters to be ≈ 0.5 m. The optimum Rayleigh length for a seed focused at the undulator entrance is therefore found to be $Z_{R\ opt} \approx 2L_g$. For this optimum focusing the seed beam waist at the injection point, $z = 0$ (beginning of PU1), is 4.1 mm. If it is assumed that a full aperture at the injection point of six times the beam radius is required to minimise diffraction effects, then a vacuum vessel aperture of ≈ 25 mm (magnetic gap minus 3mm) is sufficient. This is achieved with the step-tapered vacuum vessel design, as discussed above.

The above results show that the output power at the end of VU5 reduces as the seed waist size at the entrance to VU1 increases. (Consequently the seed radius at the injection point also decreases.) The reduced coupling between radiation and electrons with increasing radiation waist means that saturation is not achieved in the fixed undulator length. Nevertheless, it may be beneficial to use a larger seed waist size than the optimum value of 200 μm and compensate for the increased saturation length by focusing the seed into the previous module PU8 for example. (This will have no effect on the saturation power which is independent of seed.) A larger waist size will reduce output power fluctuation due to seed source pointing stability. While this will be investigated further in future design work, the current conclusion shows that the optimum seed focusing geometry may be obtained with the use of the proposed step-tapered vacuum vessel.

Variable polarisation

As has been noted above, the HHG seed sources are linearly polarised. However, this should not present problems in generating variable polarisation. When the HHG seed is injected into a planar undulator it causes the electrons to bunch in the axial (\hat{z}) direction. The polarisation of the radiation emitted is determined by the electron trajectory. Hence, if the electron bunching is initiated in a planar

undulator and subsequently transferred into an elliptically polarised undulator, the electrons will emit elliptically polarised radiation and progress via the FEL interaction to saturation. If the linearly polarised HHG seed is injected with the electrons directly into an elliptically polarised undulator then coupling between seed and electrons will occur in the plane of the radiation electric field and will begin to bunch the electrons. The bunching electrons will then emit with the elliptical polarisation determined by the undulator. Optimal coupling will occur when the major axis of the elliptically polarised undulator is co-incident with that of the electric field polarisation of the seed.

Timing

Detailed discussion of synchronisation and timing jitter effects between the seed and electron pulse at the entrance to the XUV-FEL are summarised here and presented in more detail in [1, 14]. A relation between a timing offset Δt and the peak electron current has been used with the Xie formulae [7] to estimate the effects of timing offset upon the saturation length and saturation power of the XUV-FEL operating at 100 eV. From these estimates a 50 fs offset increases the saturation length by $\sim 1.3\%$, and decreases the saturation power by $\sim 4\%$. A 100 fs offset increases the saturation length by $\sim 5\%$, and decreases the saturation power by $\sim 13\%$. Genesis simulations have also been used to investigate the effect of timing offset and are in very good agreement. While timing jitters of ~ 100 fs should be readily achievable, it is projected that this figure may be reduced to the low tens of femto-second level. It may be possible to offset the effect of the increase in saturation length by allowing the amplifier sufficient length to oversaturate. In this way the saturated power will nearly always be attained. This area is the subject of future design and research effort.

CONCLUSIONS

The main use of HHG in 4GLS is to act as a seed source for the XUV-FEL. These sources have enabled a robust conceptual design for the XUV-FEL to be developed. Established theory and simulation codes predict this FEL will generate photons of giga-watt power levels in pulses of duration 40-60 fs FWHM. The design specification presented here is optimised for 10-100 eV operation but it has been demonstrated [1] that extension to a revised photon energy range of 8-100 eV requires only small parameter changes. The quality and tunability of the HHG seed ensures the FEL remains continuously tunable generating pulses that will have very good temporal and spatial coherence with time-bandwidth products close to the Fourier transform limit for a Gaussian pulse. The XUV-FEL interaction here is acting as a simple, bandwidth limited amplifier - so long as the radiation input seed pulses have sufficient spectral purity, the output radiation is very nearly a simple amplified version of the input.

HHG sources have also been included in the 4GLS conceptual design as user sources in their own right. This has not been discussed, but is of significant importance to the overall concept of 4GLS as a facility providing multi-colour synchronised sources to the user.

It has been demonstrated that the multi-harmonic content of the HHG seed need not be filtered before injection as the gain-bandwidth of the FEL interaction ensures that only the resonant harmonic affects the FEL output.

The most critical aspect to ensuring the success of the XUV-FEL design is in the spatio-temporal synchronisation between electron pulses and HHG seed at the beginning of the FEL interaction region. While initial study suggests this is feasible, this and other aspects will now be the subject of greater scrutiny as the 4GLS project enters the technical design phase.

REFERENCES

- [1] *4GLS Conceptual Design Report*, Council for the Central Laboratory of the Research Councils, UK (2006), available from: <http://www.4gls.ac.uk/documents.htm#CDR>
- [2] *The Science Case for 4GLS* (2001), available from: http://www.4gls.ac.uk/Documents/EPSRC-Dec2001/Science_Case.pdf
- [3] M.W. Poole and B.W.J. M^cNeil, Nucl. Inst. Meth. Phys. Res. A **507**, 489 (2003)
- [4] M.W. Poole and B.W.J. M^cNeil, Proceedings of the 25th International Free Electron Laser Conference, Tsukuba, Japan (2003)
- [5] B.W.J. M^cNeil, G.R.M. Robb, N.R. Thompson, J. Jones, M.W. Poole and C.K.M. Gerth, Proceedings of the 27th International Free Electron Laser Conference, Stanford, JA-CoW / eConf C0508213 (2005)
- [6] B.W.J. M^cNeil, N.R. Thompson, and B. Sheehy, *The Conceptual Design of the 4GLS XUV-FEL*, *ibid.*
- [7] Ming Xie, Proc. Of 1995 Part. Accel. Conf., 183 (1996)
- [8] S. Reiche, Nucl. Inst. Meth. Phys. Res. A, **429**, 243, (1999)
- [9] B. Sheehy, J.A. Clarke, D.J. Dunning, N.R. Thompson, and B.W.J. M^cNeil, Proceedings of the 37th ICFA Advanced Beam Dynamics Workshop on Future Light Sources, Hamburg, Germany (2006)
- [10] See e.g. Eiji J. Takahashi et al., IEEE Journal of Selected Topics in Quantum Electronics **10**, 1315 (2004)
- [11] K.J. Schafer, B. Yang, L.F. DiMauro, and K.C. Kulander, Phys. Rev. Lett. **70**, 1599 (1993)
- [12] P.B. Corkum, Phys. Rev. Lett. **71**, 1994 (1993)
- [13] See e.g. Pascal Salieres, Anne LHuillier, Philippe Antoine and Maciej Lewenstein, Adv. At. Mol. Opt. Phys. **41**, 83 (1999)
- [14] D. Dunning et al., *First Tolerance Studies for the 4GLS FEL Sources*, *ibid.*